

Influence of positional correlations on the propagation of waves in a complex medium with polydisperse resonant scatterers

Valentin Leroy*

Laboratoire MSC, Université Paris-Diderot, CNRS (UMR 7057), Paris, France

Anatoliy Strybulevych and John H. Page

Department of Physics & Astronomy, University of Manitoba, Winnipeg, Canada

Martin G. Scanlon

Department of Food Science, University of Manitoba, Winnipeg, Canada

(Dated: February 24, 2024)

We present experimental results on a model system for studying wave propagation in a complex medium exhibiting low frequency resonances. These experiments enable us to investigate a fundamental question that is relevant for many materials, such as metamaterials, where low-frequency scattering resonances strongly influence the effective medium properties. This question concerns the effect of correlations in the positions of the scatterers on the coupling between their resonances, and hence on wave transport through the medium. To examine this question experimentally, we measure the effective medium wave number of acoustic waves in a sample made of bubbles embedded in an elastic matrix over a frequency range that includes the resonance frequency of the bubbles. The effective medium is highly dispersive, showing peaks in the attenuation and the phase velocity as functions of the frequency, which cannot be accurately described using the Independent Scattering Approximation (ISA). This discrepancy may be explained by the effects of the positional correlations of the scatterers, which we show to be dependent on the size of the scatterers. We propose a self-consistent approach for taking this “polydisperse correlation” into account and show that our model better describes the experimental results than the ISA.

PACS numbers: 43.35.+d, 43.20.+g

I. INTRODUCTION

Propagation of waves in complex media continues to be a very active subject of research. Of particular interest are complex media containing scatterers with resonances at low frequencies. Indeed, when the wavelength is large compared to the typical size of the inhomogeneities, one can use an effective medium approach, *i.e.*, consider that the wave propagates as it would do in a homogeneous medium with an effective wavevector whose value is related to the composition and the structure of the material. In most cases, the effective medium has properties that are close to the average of that of its components. But when there are resonant scatterers, their contribution to the wave field can be strong enough to significantly alter the propagation. In some cases, the effective media show intriguing properties, such as a negative refractive index, which are not encountered in nature; such materials are called *metamaterials* [1–4].

One of the key issues for wave propagation in strongly scattering materials is the effect of coupling between the scatterers near resonance, an effect that makes the traditional independent scattering approximation (ISA) inadequate. Indeed, when the resonances are strong and/or the concentration of scatterers high, positional corre-

lations and multiple scattering loops may have a non-negligible contribution. To gain a better understanding of the underlying physics, experiments on a well-controlled system with strong resonances are needed. One such system can be found in acoustics, where bubbly liquids are often regarded as model systems for the study of wave propagation with low frequency resonances. Indeed, air bubbles in a liquid have a particularly low resonance, known as the Minnaert resonance, with an angular frequency given by

$$\omega_M = \frac{v_1 \sqrt{3\rho_1/\rho_0}}{R},$$

where R is the bubble radius, v_1 is the velocity of longitudinal waves in air, and ρ_1 and ρ_0 are the mass densities of the air and the liquid, respectively. As the ratios of the densities and the velocities are small, it is easy to see that this resonance is at very low frequency:

$$\frac{\omega_M R}{v_0} = \sqrt{3\rho_1/\rho_0} \frac{v_1}{v_0} \ll 1.$$

Here, v_0 is the longitudinal sound velocity in the liquid. This equation shows that, at resonance, the wavelength is large compared to the bubble size. This is important because, then, at the resonance frequency, not only is the response of the bubble strong, but several bubbles (and potentially many) can be driven in phase, thus yielding a collective constructive contribution to the pressure field. This explains why a minute quantity of gas bubbles can

*Electronic address: valentin.leroy@univ-paris-diderot.fr

dramatically change the effective acoustic properties of a liquid.

If the bubble is no longer in a liquid, but in an elastic medium with shear velocity u_0 , its resonance frequency becomes [5, 6]:

$$\omega_M = \frac{\sqrt{3v_1^2\rho_1/\rho_0 + 4u_0^2}}{R}, \quad (1)$$

so the same condition of small radius with respect to wavelength persists as long as the elastic medium is a soft solid in which $u_0 \ll v_0$. As a result, elastic bubbly media are also good candidates as model systems for investigating wave propagation in the presence of low frequency resonances. In addition, they offer two practical advantages compared to bubbly liquids: (1) bubbles do not move, which means that a precise knowledge of their positions can be obtained; (2) the frequency of the resonance can be shifted by tuning the shear velocity in the elastic matrix. Bubbly soft media with negligible shear velocity have already been studied [7–9], and the ISA was found to reliably predict the experimental results, at least for concentrations of bubbles up to 1%. The present article focuses on a bubbly polydimethylsiloxane (PDMS) sample, in which the shear modulus is expected to significantly change the bubble’s response to the incident ultrasonic field and the propagation of waves in the medium. Our aim is to see if the ISA is still relevant in this case. Beyond the fundamental aspect of the study, and the potential applications for design of metamaterials, it should be noted that a better understanding of the acoustic properties of bubbly elastic media is interesting *per se*, since many practical applications, in the medical or the food science fields for instance, involve the presence of bubbles in a soft elastic matrix.

The present paper is organized as follows. The next section gives a brief overview of the ISA, with a focus on its application to acoustic propagation in bubbly media. Then we describe how our bubbly samples were made and characterized. Section IV reports the experimental measurements of velocity and attenuation in one typical sample, and compares the experimental results with the ISA. Two main limitations of the model are also discussed: the assumption of sample homogeneity on length scales larger than the scatterer size (e.g., gradients in the concentration of the scatterers) and the neglect of correlations in the positions of the scatterers. Methods for overcoming these limitations are proposed.

II. THE INDEPENDENT SCATTERING APPROXIMATION

Based on a diagrammatic representation of scattering events [10], the ISA predicts the following effective wavenumber k for a medium with n scatterers per unit volume defined by their scattering function f_s :

$$k^2 = k_0^2 + 4\pi n f_s, \quad (2)$$

where k_0 is the wavenumber in the pure medium (matrix). The ISA is actually equivalent to the model developed, with another approach, by Foldy in 1945 [11]. In the following, we will use equally “ISA” or “Foldy’s model” when referring to equation (2).

In eq. (2), the effect of the scatterers on propagation in the pure medium is described by a term proportional to $n f_s$, *i.e.*, a simple addition of the individual scattering events, which are assumed to be independent. Models have been proposed for incorporating either the correlations between the scatterings [12] or the loops, *i.e.*, the events in which the same scatterer or spot inside the sample is visited more than once by the wave [13, 14]. We discuss only the ISA in this section, since it is the simplest model and it gives reasonable predictions of wave transport in many cases. We will introduce later, in section IV C and the appendix, extensions to the ISA for dealing with the positional correlations of the scatterers.

Equation (2) considers a monodisperse assembly of scatterers. In practical applications, one is often dealing with polydisperse media, in which case the ISA predicts that

$$k^2 = k_0^2 + \int 4\pi n(R) dR f_s(R), \quad (3)$$

where $n(R)dR$ is the number of bubbles per unit volume whose radius is between R and $R + dR$, and $f_s(R)$ is the scattering function for a scatterer of radius R .

Let us apply the ISA to a bubbly medium. When the scatterer is a bubble, its isotropic scattering function is given by

$$f_s(\omega, R) = \frac{R}{(\omega_M/\omega)^2 - 1 + i\delta}, \quad (4)$$

where δ is the damping constant due to thermal, viscous and radiative losses [15] and ω_M the resonance angular frequency given by Eq. (1), which can be written

$$\omega_M^2 = \frac{3\kappa P_1 + 4\mu'}{\rho_0 R^2}, \quad (5)$$

with κ the polytropic index for the transformations undergone by the gas [15] ($\kappa = 1.4$ for air), P_1 the pressure of the gas in the bubbles, ρ_0 the mass density of the matrix, and μ' the real part of the shear modulus of the matrix. Surface tension effects are negligible for the bubble size considered in our experiments. Mode conversion is not considered in this model since it has been shown to be negligible for this system on account of the large difference between the shear modulus of the matrix and the longitudinal one ($u_0 \ll v_0$) [16]. Hence the only significant contribution of the nonzero shear modulus is its effect on the resonance frequency of the bubble, which is increased by the stiffness of the matrix. Another approximation we make is to reduce the scattering function to its isotropic component, neglecting the dipolar and higher contributions. This approximation is generally good when the wavelength is large compared to the

size of the scatterers, and it will be shown to be accurate for describing our experiments.

In figure 1, we give two examples of the effective attenuation and velocity as functions of the frequency, as calculated by Foldy's model. For the sake of generality, we consider log-normal distributions of bubble size:

$$n(R) = \frac{n_0}{\sqrt{2\pi}\epsilon R} \exp\left(-\frac{(\ln R/R_0)^2}{2\epsilon^2}\right), \quad (6)$$

where R_0 is the median radius, ϵ the width of the distribution, and n_0 the bubble concentration. Note that for distributions that are not too broad ($\epsilon < 0.2$), log-normal distributions are close to normal distributions: then R_0 and ϵ can be viewed as the mean radius and coefficient of variation (*i.e.*, standard deviation divided by the mean), respectively. The latter quantity, which we will refer to as the polydispersity factor, measures the range of bubble sizes in the distribution. The bubble concentration n_0 is related to the gas volume fraction Φ by

$$n_0 = \frac{3\Phi}{4\pi R_0^3 \exp(9\epsilon^2/2)}. \quad (7)$$

The bubble size distribution in Fig. 1 is described by $R_0 = 150 \mu\text{m}$, $\epsilon = 25\%$ and $\Phi = 2\%$. Two host media are considered: water (dashed lines), and an elastic matrix with $\mu' = 0.7 \text{ MPa}$, $\mu'' = 0.4 \text{ MPa}$ (solid lines). For both media, very dispersive behavior is predicted: the attenuation and velocity show peaks, which occur at higher frequencies in the elastic medium.

At low frequencies ($\omega < \omega_M$), sound propagation in the bubbly medium is weakly attenuated, and its very low phase velocity is accurately predicted by Wood's relation [17], modified to account for the elastic effects. For $5 \times 10^{-4} < \Phi < 10^{-1}$, this relation can be approximated (within 5%) as

$$v_{\text{lf}} \simeq \sqrt{\frac{\kappa P_1 + 4\mu'/3}{\rho_0 \Phi}}, \quad (8)$$

where P_1 is the pressure of the gas in the bubbles and ρ_0 the density of the matrix. Eq. (8) gives, in our example, $v_{\text{lf}} = 122$ and 248 m/s in water and the elastic matrix, respectively.

Near the Minnaert frequencies of the bubbles, the acoustic waves are highly attenuated by the bubbly medium: the attenuation reaches a peak α_{max} at frequency f_{max} , corresponding to the resonance frequency for a monodisperse distribution. In water, the peak is very sharp and associated with the bubble resonances ($f_{\text{max}} = 22 \text{ kHz}$ as expected by Eq. (5) for a $150\text{-}\mu\text{m}$ -radius bubble). Eqs. (2) and (4) give the physical origin of this sharp peak: at resonance, the scattering function f_s is large and imaginary, which leads to a large imaginary part of the effective wave number k . This sharp resonant effect is followed by a broader regime (roughly 60-400 kHz in our example) in which the attenuation is still large. This is explained by the negative response of

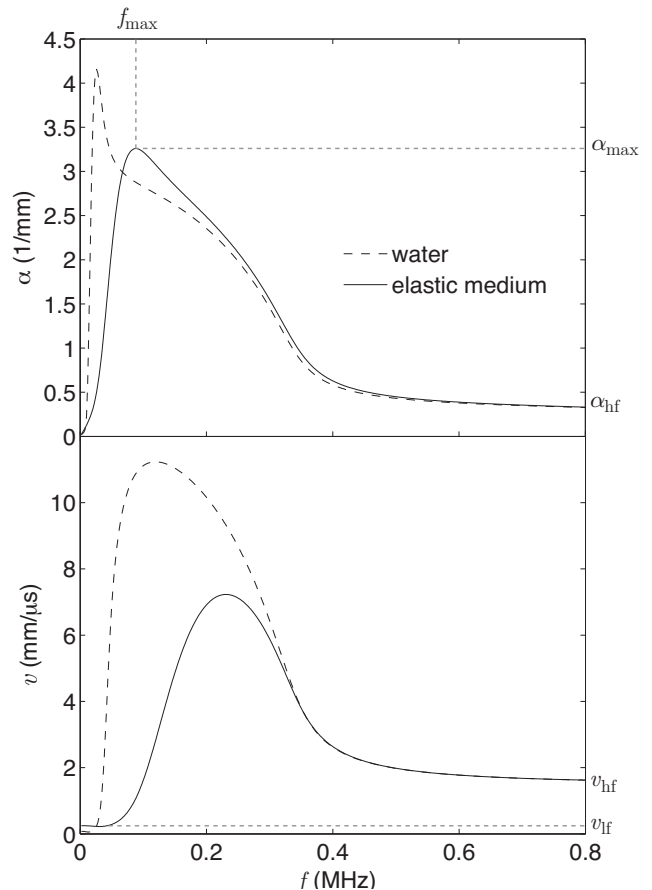


FIG. 1: (Color online) Predictions of the ISA for the attenuation α (top) and phase velocity v (bottom) as functions of frequency for bubbles in water (dashed lines) and in an elastic matrix (solid lines) with $\mu' = 0.7 \text{ MPa}$, $\mu'' = 0.4 \text{ MPa}$; the bubble concentration is 2% and the mean radius is taken to be $150 \mu\text{m}$ with a 25% polydispersity. The characteristic features (f_{max} , α_{max} , α_{hf} , v_{lf} , and v_{hf}) are indicated.

the bubbles. Indeed, when driven at a frequency higher than its resonance frequency, a bubble has a scattering function which reduces approximately to $f_s = -R$ when $\delta \ll 1$ (see Eq. (4)). Even though the bubble is not resonating, its contribution is far from negligible. Indeed, one can rewrite Eq. (2) as

$$k^2 = k_0^2 \left(1 - \frac{R\lambda^2}{\pi d^3}\right), \quad (9)$$

where d is the typical distance between bubbles. As long as the wavelength is large compared to this distance ($\lambda/d \gg 1$), the square of the effective wavenumber is negative: waves are evanescent. In our example of 2% bubbly water with $150 \mu\text{m}$ -radius bubbles, the typical distance between bubbles is 0.9 mm , which means that $R\lambda^2/(\pi d^3) > 1$ for $f < 380 \text{ kHz}$.

In our example of an elastic medium, the high viscosity (μ'' of 0.4 MPa corresponds, at 0.1 MHz , to a viscosity 640 times larger than that of water) tends to damp the

oscillations of the bubbles at resonance, so the attenuation peak is lower and less sharp (see figure 1). As a paradoxical consequence, the more viscous the medium in which bubbles are embedded, the lower the maximum of attenuation of sound. Note that the sharp peak of attenuation also disappears when the bubble size distribution is too broad. Interestingly, even if the resonant effects are too weak to give rise to significant resonant attenuation, they still lead to an evanescent regime. In this case, the position of the attenuation peak does not correspond to the resonance of the average size bubbles, but rather to a frequency that is just above the resonance frequency of the small bubbles of the distribution, as it corresponds to all the bubbles being driven at a frequency higher than their resonance frequencies. For instance, in our example $f_{\max} = 90$ kHz for the bubbly elastic medium, which corresponds to a radius of $100 \mu\text{m}$ according to Eq. (5).

When the resonances are smoothed out, an approximate formula can be established for the maximum of the attenuation:

$$\alpha_{\max} = \frac{2\sqrt{3\Phi}}{R_0 \exp(2\epsilon^2)}, \quad (10)$$

which has the benefit of depending only on the bubble concentration and size distribution (not on either the damping constant of the bubbles or the shear modulus of the matrix).

At higher frequencies, the evanescent regime disappears: the attenuation and velocity reach constant values, which can be approximated by:

$$\alpha_{\text{hf}} = \frac{3\Phi}{R_0 \exp(5\epsilon^2/2)}, \quad (11)$$

$$v_{\text{hf}} = v_0. \quad (12)$$

Interestingly, if Foldy's model applies, one can determine the 5 parameters Φ , R_0 , ϵ , μ' , and v_0 from the measurement of the 5 quantities v_{lf} , f_{\max} , α_{\max} , α_{hf} , and v_{hf} in a bubbly medium.

III. MATERIALS AND METHODS

A. Sample preparation

Samples were prepared by mixing 100 g of RTV 615 (GE Silicones, 90 g monomers and 10 g hardener) in a 600 mL beaker with a Sorvall Omni Mixer (Ivan Sorvall, Inc., Norwalk, CT; nominal operating speed 16,000 rpm) for 1 minute to incorporate bubbles. Then, after waiting for an interval of 10-20 minutes for the biggest bubbles to rise and disappear, the bubbly liquid was poured into a cell (thickness 2.6 mm, diameter 11 cm), which was rotated at 5 rpm to prevent creaming (bubbles rising to the top of the container). At room temperature, a solid sample was obtained in 1 day.

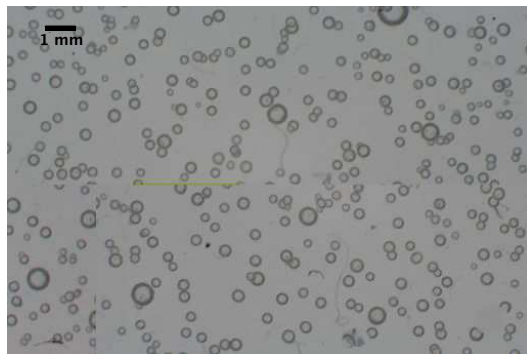


FIG. 2: (Color online) Example of an image taken for the bubble size analysis (optical characterization).

B. Sample characterization

Testing of Foldy's model requires that some of the parameters of the sample are known: the bubble size distribution ($n(R)$), the matrix rheology (μ) and the velocity of sound in the matrix (v_0).

a. Optical characterization was made by taking pictures at different positions in the sample. The depth of field was larger than the thickness of the sample, which means that the total volume of the image was known ($16 \times 11 \times 2.6 \text{ mm}^3$). A typical image is shown in figure 2; the contrast was good enough for an automatic size analysis to be performed (ImageJ). The radius measurement was possible with a one pixel accuracy, *i.e.*, $5 \mu\text{m}$. A total of 839 bubbles was analyzed. To avoid biased measurements of big bubbles, overlaid bubbles were excluded from the size analysis. However, the total number of bubbles was determined (1098) for a correct estimation of the bubble volume fraction, assuming the same size distribution for the overlaid bubbles. The radius distribution was centred around $165 \pm 5 \mu\text{m}$ with a polydispersity of $21 \pm 1\%$ and a volume fraction of $2 \pm 0.2\%$ (see histogram in figure 3).

b. Rheological characterization was necessary to measure the shear modulus over the frequency range used for the ultrasonic experiments (30-800 kHz). We used a shear wave reflection technique (see [18] or [19] for details) to measure the complex shear modulus $\mu = \mu' + i\mu''$ from 300 to 500 kHz. For lower frequencies (around 30 kHz) an estimation of μ was possible by measuring the acoustic response of a single bubble (see [20] for a description of the technique). Over the 30-500 kHz frequency range, our measurements are consistent with the following behaviour of the real (μ') and imaginary (μ'') parts of the shear modulus:

$$\mu' = 0.6 + 0.7 \times f, \quad (13a)$$

$$\mu'' = 0.2 + 1.8 \times f, \quad (13b)$$

where the moduli are in MPa and the frequency f in MHz. Equations (13) only give the order of magnitude of the shear modulus for a given RTV615 sample. In-

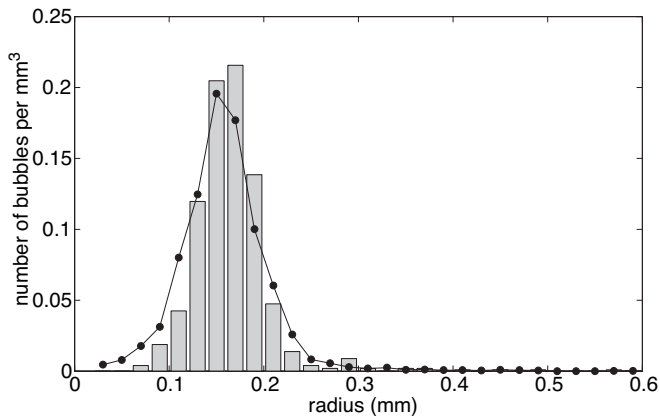


FIG. 3: (Color online) Histogram of the bubble radius distribution for the sample in figure 2, obtained from the image analysis. The superposed curve (circles plus connecting lines) corresponds to the result of the x-ray tomography analysis.

deed, the precise protocol used for preparation, such as the temperature and time of the hardening process for instance, may have a non-negligible impact on the modulus [21]. As a consequence, deviations from the predictions of Eqs. (13) can be observed for a given sample.

The stationary limit ($f = 0$ MHz) of our estimate of μ' is in good agreement with the value reported in the literature [21].

c. Ultrasonic characterization was also performed by standard techniques [8] to measure the velocity and attenuation of sound in the *pure* PDMS. The longitudinal velocity was found to be constant over the frequency range investigated (30 kHz - 5 MHz): $v_0 = 1.02$ mm/ μ s, in accordance with previously reported values [22]. For the attenuation, the following law was found: $\alpha_0 = 0.023f^{1.54}$ mm $^{-1}$ (with frequency f in MHz).

d. X-ray characterization. To investigate the spatial distribution of the bubbles in one of the samples, x-ray tomography images were acquired, using an Xradia MicroXCT 3D x-ray transmission microscope (18 μ m/px). After the ultrasonic measurements, the sample was cut in pieces small enough to fit in the apparatus ($7.5 \times 10 \times 2.6$ mm 3), and 21 pieces were imaged, for a total of 3700 bubbles. A software program was written to enable the reconstruction of the 3D structure of each piece: for every bubble i , its radius R_i and position $[x_i, y_i, z_i]$ were determined with 1 pixel accuracy. The size distribution was determined and successfully compared to the results of the optical characterization: we found a mean radius of 160 ± 18 μ m with a polydispersity of 25 ± 1 % and a volume fraction of 2.2 ± 0.3 % (see figure 3 and table I). Moreover, the 3D data gave insight into the homogeneity of the sample, as well as on the correlations in the bubble positions, as described in sections IV B and IV C.

TABLE I: Parameters of the bubble size distribution, extracted from the optical and x-ray measurements.

	volume fraction Φ (%)	average radius $\langle R \rangle$ (μ m)	polydispersity $\frac{\sqrt{\langle R^2 \rangle - \langle R \rangle^2}}{\langle R \rangle}$ (%)
optics	2.0 ± 0.2	165 ± 5	21 ± 1
x-ray	2.2 ± 0.3	160 ± 18	25 ± 1

C. Ultrasonic measurements

The acoustic properties of the samples were measured with the following set-up. In a large tank ($60 \times 60 \times 120$ cm 3) filled with reverse osmosis water, a piezoelectric transducer generated a pulse that propagated through water, traversed the sample and was detected by a hydrophone. Because the attenuation in the sample was large, and because the divergence of the beam was not negligible (especially at low frequencies), the use of a screen was essential to reduce spurious signals. The aperture of the screen (6 cm) was larger than the wavelength of the pulse (3.75 cm at 40 kHz) to limit diffraction effects, but smaller than the diameter of the sample (11 cm).

Gaussian pulses, with central frequencies ranging from 40 to 600 kHz, were generated by an Arbitrary Wave Generator, and three different transducers, having central frequencies of 100, 250 and 500 kHz, were used to cover the range of frequencies. The pulses were recorded, with a hydrophone, in two different cases: when the sample was mounted on the screen ($s_1(t)$), and when the sample was absent ($s_2(t)$). The signals were averaged over 100 acquisitions when the attenuation was low (for reference measurements, for example), and up to 5000 acquisitions for highly attenuated signals. Signals $s_1(t)$ and $s_2(t)$ were then truncated to eliminate spurious echoes, and Fourier transformed into $S_1(\omega)$ and $S_2(\omega)$ respectively. Then, $T(\omega)$, the ratio of the transmission with and without the sample in the path of the acoustic beam at a given angular frequency, was calculated.

For an incoming plane monochromatic wave $\exp(ikx - i\omega t)$, $T(\omega)$ is given by

$$T(\omega) = \frac{4ZZ_w}{(Z_w + Z)^2} \times \frac{e^{i(k-k_w)d}}{1 - \left(\frac{Z-Z_w}{Z+Z_w}e^{ikd}\right)^2}, \quad (14)$$

where k and k_w are the wave numbers in the sample and in the water respectively, Z and Z_w the acoustic impedances, and d the thickness of the sample. Because the impedance Z depends on k ($Z = \rho\omega/k$, with ρ the mass density of the sample), equation (14) is not directly invertible to extract k : an iteration method was used [8]. From k , the phase velocity $v = \omega/\text{Re}(k)$ and the attenuation $\alpha = 2\text{Im}(k)$ can be calculated. Error-bars on the measurements were evaluated by taking into account the following sources of uncertainty: thickness of the sample,

noise in the Fourier transforms, truncation of the time pulse.

An important issue in measuring the acoustic properties of a medium is the statistical relevance of results for a single sample. Theories predict the average properties, *i.e.*, what one can measure when averaging over different samples having the same general parameters. To obtain insight on this issue, we measured the transmitted signal not only in the centre of the acoustic beam, but also on a 7×7 grid with a 5 mm step. From this scanning, a “typically averaged signal” could be obtained (with correction for the geometrical differences), and this was compared to the centre pulse.

IV. EXPERIMENTAL RESULTS AND DISCUSSION

Several bubbly PDMS samples were tested, with different void fractions (0.5-3.5 %) and polydispersities (20-50 %), but with the same average radius (around $150 \mu\text{m}$). In this article, we focus on representative results obtained with one selected sample, which was characterized by x-ray tomography. Figure 4 shows the measured attenuation and phase velocity in the sample as functions of the frequency. The general aspect of the curves follows what one would expect for a bubbly medium (see figure 1): both the attenuation and the velocity exhibit peaks in frequency with very large values at their maxima (3.5 mm^{-1} and $4.5 \text{ mm}/\mu\text{s}$, respectively), the velocity is low ($0.26 \text{ mm}/\mu\text{s}$) at low frequencies, and close to the value in the pure PDMS at higher frequencies. Note that two cases are considered: when only one pulse is analysed (open circles) and when the average is made over the 49 positions of the hydrophone (solid circles). Except for the peak in velocity, both analyses give similar results. It indicates that substantial information can be obtained from a single pulse measurement, which is interesting for practical purposes. Note that measurements are difficult when the velocity is high because small time shifts have to be extracted from the phase shift which is dominated by the complex impedance rather than the transit time.

The five typical quantities introduced in section II can be measured and compared to equations (5), and (8)-(12), calculated with the parameters found in section III B. As shown in table II, the agreement is rather satisfying: f_{max} and α_{hf} are within 10% and the other quantities within 20%. Note that for v_{lf} and v_{hf} the measured values may not correspond exactly to the asymptotic values because of the limited range of frequencies in the measurements.

A. Comparison with ISA

Figure 5 offers a further step in the comparison process. Predictions of the ISA model are plotted as dotted lines.

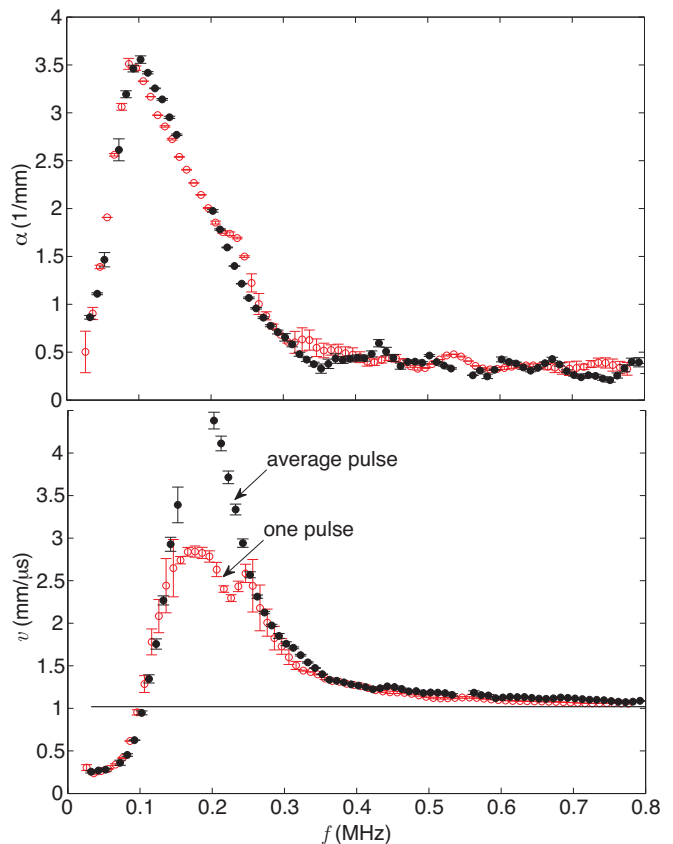


FIG. 4: (Color online) Attenuation α and phase velocity v in the bubbly PDMS sample, measured from a single pulse (open circles) and from an average pulse (solid circles). The velocity in the pure PDMS is shown by the solid line. The attenuation in pure PDMS is, on average, 2 orders of magnitude less than in the bubbly sample (too small to be visible on the graph).

TABLE II: Five characteristic quantities measured experimentally (first line), and predicted by the model (second line).

	f_{max} (kHz)	α_{max} (mm^{-1})	α_{hf} (mm^{-1})	v_{lf} (m/s)	v_{hf} (m/s)
exp.	100	3.5	0.40	260	1180
mod.	90 ^a	2.8	0.35	224	1020

^aCalculated with Eq. (5) by taking the radius of the small bubbles of the distribution (*i.e.*, $100 \mu\text{m}$, see figure 3). This is appropriate since for polydisperse distributions of sizes, the peak in attenuation corresponds to the resonances of the smaller bubbles, as noted in section II.

Parameters for the model were taken as measured in section III B, the histogram measured in the x-ray experiment being chosen for $n(R)$. In the low and high limits of the frequency range, the comparison is good. However, the attenuation and velocity peaks are not correctly predicted: their frequencies and amplitudes are both smaller than the experimental data. Note that this discrepancy

was observed for all the samples we investigated. The comparison is slightly better when the dipole terms in the bubbles' responses are considered (solid lines) but the discrepancy in the peaks' positions and magnitude is still large. Higher order scattering has negligible contributions.

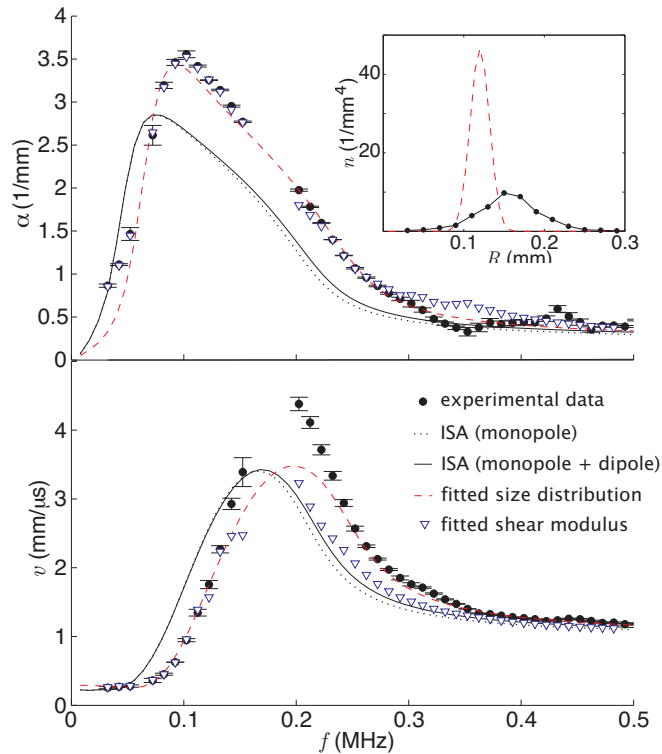


FIG. 5: (Color online) Close-up of the attenuation and velocity peaks. Solid circles correspond to experimental data (same as in Fig. 4). Comparison with Foldy's model is shown for monopolar scattering of the bubbles (dotted lines) and monopolar + dipolar scattering (solid lines). Note that there are no adjustable parameters in this comparison of the theory with experiment. Results of fitting the model to the data by allowing either the size distribution (dashed lines) or the shear modulus (triangles) to vary are also shown. In the inset, the size distribution determined by the x-ray experiment (solid line) is compared to the one inferred from the fit to the ultrasonic data (dashed lines).

To check whether the discrepancy could be explained by the uncertainty in the measured size distribution, we determined the $n(R)$ function that was needed to achieve a better fit. As shown in the inset of Fig. 5, this leads to a totally unrealistic distribution, with smaller bubbles (mean radius $120 \mu\text{m}$), a narrower distribution (10% polydispersity), and a smaller void fraction (1.1%). One can understand why such a size distribution is obtained by looking at equation (2). If the peaks are at too low frequencies and with too low amplitudes, it means that the nf_s term is not high enough compared to k_0^2 , *i.e.*, that the bubble contribution is too weak. A way of fixing this is to consider smaller bubbles, in order to shift the resonance

to higher frequencies, and to increase the number of bubbles per unit volume to magnify their contribution. This explains the difference between the fitted and the actual size distribution in figure 5 inset. An important practical application is that if one uses Foldy's model for fitting the experimental data, an incorrect bubble size distribution will be obtained. Note that the same phenomenon was observed for bubbles in bread dough, with the same trend of Foldy's model predicting bubbles smaller than those determined from x-ray measurements [23].

Another possible source of error was the shear modulus, whose measurement was not very precise. For each frequency, we determined the complex shear modulus that gave the best fit to the experimental data. As shown by the triangles in Fig. 5, a good fit was possible for the attenuation. For the velocity, the agreement was good for lower frequencies, but poor at higher frequencies. Moreover, as shown in figure 6, the fitting leads to unrealistic values for μ' and μ'' . Again, one can qualitatively understand these values: the real part of the fitted shear modulus is high in order to shift the peaks to higher frequencies, and the imaginary part is low (even zero) so that the oscillations of the bubbles are not damped by viscosity, and the scattering function f_s is large.

These results suggest that Foldy's model is inadequate for describing wave propagation in the PDMS sample. In the following we examine two possible explanations, and propose a model to account for these discrepancies.

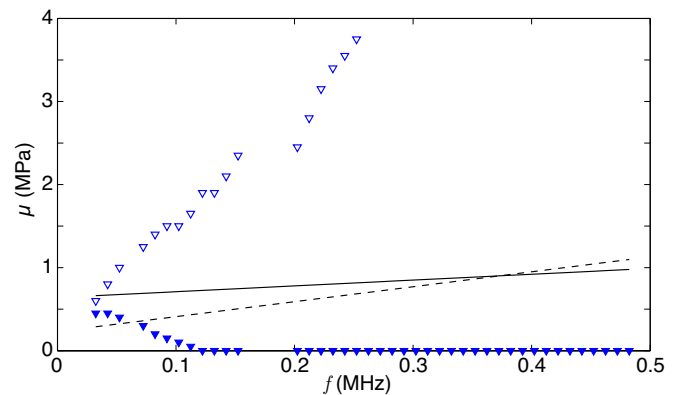


FIG. 6: (Color online) Shear moduli as functions of frequency. The lines correspond to the results for experimental μ' (solid line) and μ'' (dashed line), as given in equations (13). Open triangles show the fitted values for μ' , solid ones for μ'' .

B. Homogeneity of the sample

An important hypothesis made in all the effective medium models consists in assuming that the sample is homogeneous, *i.e.*, any part of the sample can be considered as equivalent to the others. The x-ray inspection of the sample reveals a homogeneous structure in the transverse directions, but a non-homogeneous one along

the thickness. Probably because of the upward buoyancy force exerted on the bubbles during the filling of the cell, the concentration of bubbles is varying, as shown in Fig. 7: the bottom part of the sample is free of bubbles, whereas the top part has a higher concentration. The bubble size distribution is also slightly different from one layer to the other.

We investigated the influence of this heterogeneity of the sample on the acoustic propagation. Each layer i ($1 < i < 50$) of thickness $d = 52 \mu\text{m}$ was considered as an effective medium following Foldy's model with a concentration n'/d and a bubble size distribution as measured by the x-ray tomography. Following Brekhovskikh [24], we computed the transmission through this multi-layer system, and compared it to the experimental transmission. Figure 8 shows the result: accounting for the inhomogeneity of the bubble concentration with the 50 layer model does not change the prediction much, implying that the heterogeneity of the bubble concentration plays a negligible role in acoustic wave propagation through the medium.

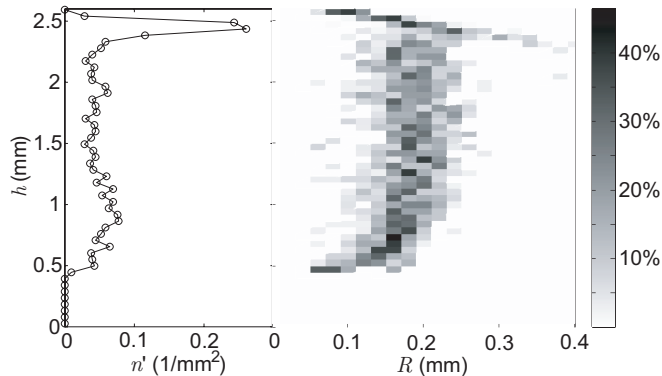


FIG. 7: (Color online) The layered structure of the sample is revealed by the x-ray tomography. Along the thickness h of the sample, we report the number of bubbles per unit area n' (left) and the radii distribution histogram (right) for each layer.

C. Positional correlations

Another approximation in Foldy's model is the assumption that the positions of the scatterers are uncorrelated. Recent experiments in a 2D system of steel rods in water have shown that Keller's approach results in a very good correction to the model when correlations needed to be included [25]. In Keller's approach, the effective wave vector is related to the correlation function by:

$$k^2 = k_0^2 + 4\pi n f_s - (4\pi n f_s)^2 \int (1 - g(r)) \frac{\sin kr}{k} e^{ik_0 r} dr \quad (15)$$

where the correlations are taken into account by a radial function $g(r)$ such that the local concentration of scat-

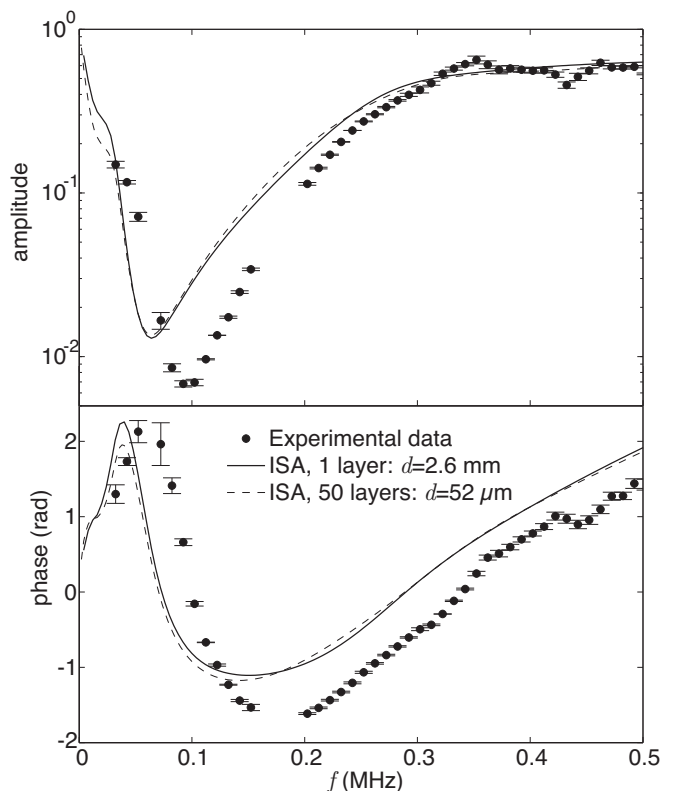


FIG. 8: (Color online) Amplitude (top) and phase (bottom) of the acoustic transmission through the sample. Because the data are the same as in figure 5, the same discrepancy between Foldy's prediction for a homogenous sample (solid lines) and the experimental data (circles) is obtained. The prediction for a layered medium (dashed lines) does not bring better agreement.

terers at a distance r from a scatterer is $n(r) = n_0 g(r)$, where n_0 is the average concentration. For point-like scatterers, $g = 1$ and Foldy's approximation is recovered. For hard spheres, $g = 0$ for $r < 2R$ and 1 at larger distances. In general, g can take more complicated forms, depending on the correlation mechanisms involved in the medium.

From the x-ray tomography data, we were able to estimate the function g for our sample. The general procedure for measuring such a function involves the following steps. First, one considers a sphere of radius r_N around one bubble and counts the number of bubbles in each spherical layer between r_i and r_{i+1} . Then, averaging over different central bubbles gives a statistical estimate of $g(r)$. However, a limit of this technique is that the bubbles chosen as centres of the spheres cannot be at less than r_N from an edge of the sample. Thus, if one wants to investigate long-range correlations by taking high values of r_N , the statistics are poor because the number of bubbles that are far enough from the borders is small. For our thin sample, this limitation was severe. To circumvent this problem, we used $1/8$ of each sphere, with

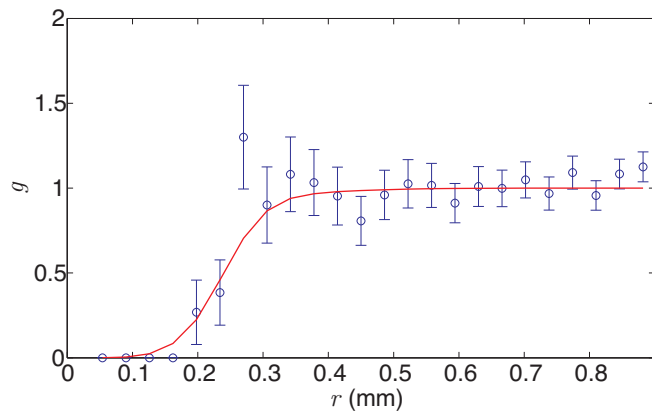


FIG. 9: (Color online) Function g as measured from the x-ray tomography data (circles). Error-bars correspond to one standard deviation. The solid line corresponds to the hard-sphere approximation for the bubble size distribution measured in the sample.

an orientation chosen so that its volume did not cross any boundaries of the sample. Figure 9 shows the result of these measurements up to a maximum distance of 0.9 mm. It appears that the g function is very similar to the predictions of the hard-sphere approximation (solid line). Note that the oscillations in the g function that are predicted by the frequently used Percus-Yevick approximation [25] are not expected to be significant here because the concentration of scatterers is low. Numerical simulations with random positions of scatterers in a box confirm that a simple hard-spheres law is a good approximation for a 2% volume fraction.

The predictions of Keller's model for the attenuation and velocity in the sample are shown in Fig. 10 for three different g functions. When the hard sphere approximation is used (*i.e.*, the solid curve of Fig. 9 is taken), one obtains the dashed lines, which only give a slightly better agreement than the ISA. From the measured correlations, we also consider the high limit (*i.e.*, the experimental points plus one standard deviation) and the low limit (*i.e.*, the experimental points minus one standard deviation) for the g function. They give different corrections: while the former gives a worse agreement, the latter improves it. One can understand this difference qualitatively by re-writing equation (15) as

$$k^2 = k_0^2 \left[1 + \frac{4\pi n f_s}{k_0^2} \left(1 - 4\pi n f_s \int (1-g)r dr \right) \right], \quad (16)$$

where the reasonable approximations $kr \ll 1$ and $k_0 r \ll 1$ have been made. It is important to note that, in the frequency range over which the discrepancy is high, the bubbles are responding in phase opposition to the pressure field, *i.e.* $\text{Re}(f_s) < 0$. So, according to equation (16), the correlations increase the effect of the bubbles on k if $g < 1$, whereas they decrease it if $g > 1$. Note that a simple criterion can be deduced from Eq. (16) to estimate

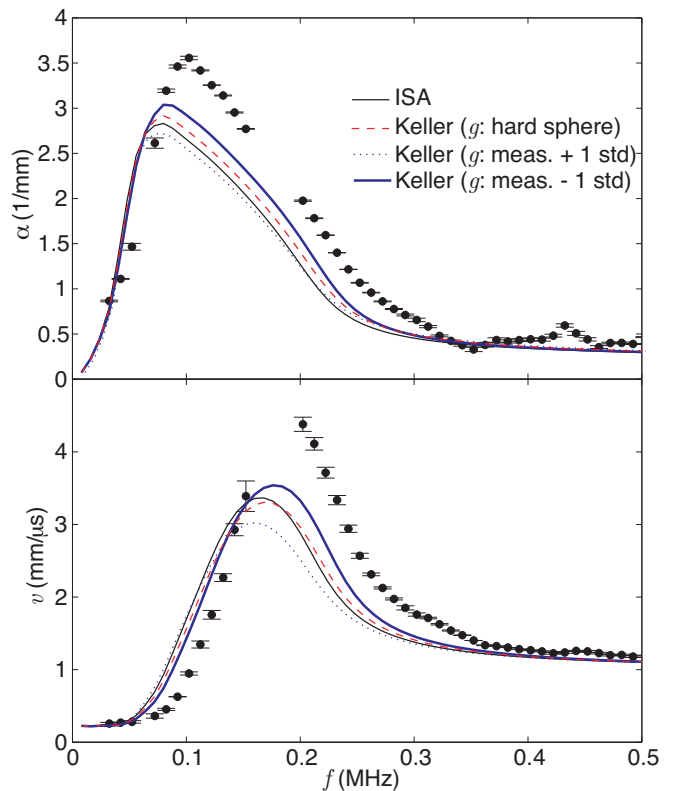


FIG. 10: (Color online) Investigation of the effect of correlations. The experimental attenuation and velocity (circles) and the ISA prediction (solid thin lines) are shown again, as in figure 4. Keller's approach (Eq. (15)) is plotted for the hard-sphere correlation (dashed lines), for the high estimation of g measured from the x-ray data (dotted lines), and for the low estimation of g (thick solid lines).

the importance of the corrections due to correlation. If g is roughly described as a step function going from 0 to 1 at distance r_c , the term with the integral in Eq. (16), which we will denote as β , reduces to

$$\beta = \frac{3}{2} \Phi \frac{f_s}{R} \left(\frac{r_c}{R} \right)^2. \quad (17)$$

Thus, the magnitude of the correction depends on the ratio of r_c to the radius of the bubbles R . Long-range correlations are thus expected to have a stronger effect.

It appears that Keller's approach, with a reasonable estimate of the g function, introduces a correction that goes in the right direction for better agreement. But the agreement is still unsatisfactory. Moreover, Keller's expression applies to a monodisperse medium, whereas our bubbly PDMS is a polydisperse sample. So far, we have assumed that the polydispersity could be taken into account by changing $n f_s$ into $\int n(R) dR f_s(R)$ in the equations. However, as we show in appendix A, a self-consistent approach provides a more general expression (see equation (A7)), in which the correlations depend on the size of the scatterer: $g(r)$ becomes $g(r, R)$. To exam-

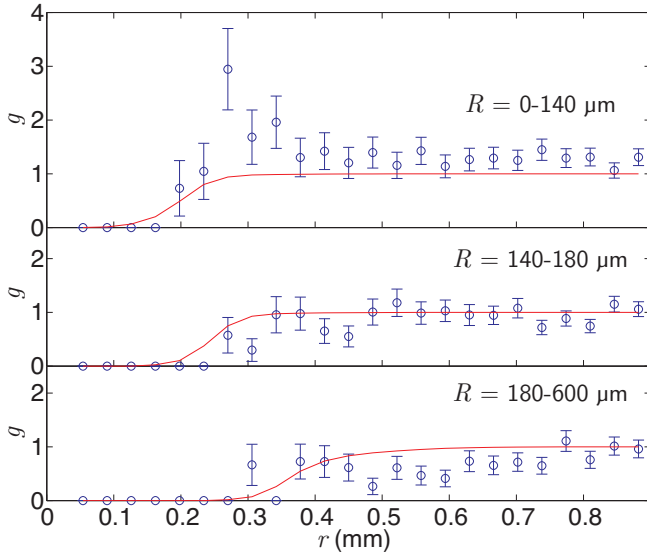


FIG. 11: (Color online) Function $g(r, R)$ as measured from the x-ray tomography data (circles) on three populations of bubble radii. Error-bars correspond to one standard deviation. The solid line corresponds to the hard-sphere approximation for the bubble size distribution measured in the sample.

ine this polydispersity effect, we considered 3 different populations of “central” bubbles: 0-140 μm , 140-180 μm , and 180-600 μm . For each population, we were able to average over approximately 1000 bubbles, ensuring good statistics. Figure 11 shows the g functions obtained for these 3 populations. For the small bubbles, there is a clear maximum of the g function. This is an indication of clusters. A close inspection of the picture in figure 2 indeed gives the impression that the small bubbles are clustered. For the average size bubbles, the g function is similar to the hard-sphere approximation. For the big bubbles, we find evidence of depletion: there is a lower probability of finding a bubble close to a big one. Again, note that the photo in Fig. 2 shows isolated big bubbles.

Figure 12 shows the predictions of our self-consistent approach (SCA) when 3 different possibilities are considered for $g(r, R)$: hard sphere approximation (solid lines in Fig. 11), and the measured values of g including the low and the high limits (bottom and top of the error bars in Fig. 11). It appears that the effects observed in Fig. 10 are amplified when the polydisperse correlation is taken into account. Interestingly, even for the hard sphere approximation, slightly better agreement is found (see table III). This can be explained by the following argument: large bubbles scatter more than small bubbles (see equation (4)), and their average correlation distance r_c is also larger.

When the range of measured values of g is considered, the agreement is better or worse, depending on whether the high or the low limit of the possible g function is considered. It follows that, given the precision of our correlation measurements, we cannot conclude whether

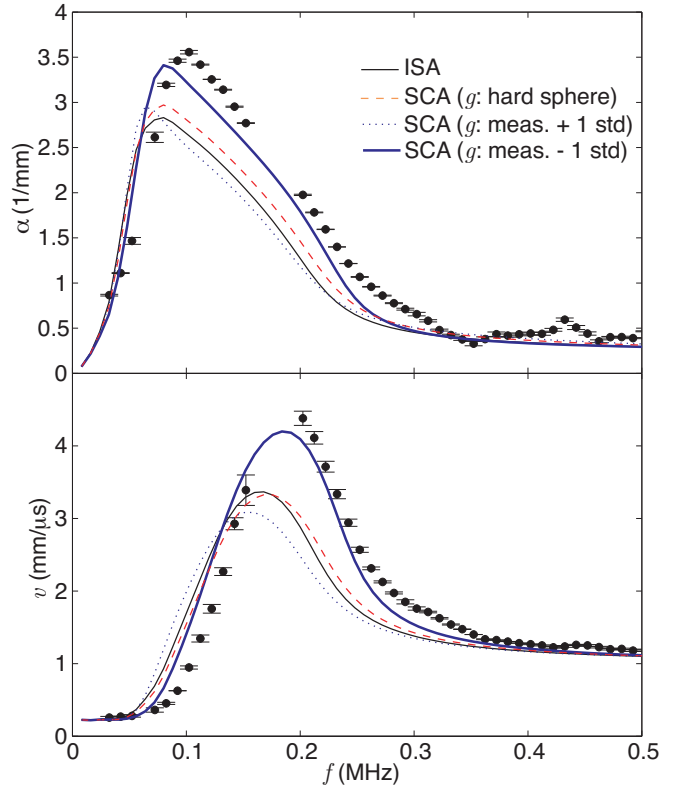


FIG. 12: (Color online) The effect of polydisperse correlations as predicted by the self-consistent approach (SCA). Three $g(R, r)$ functions are considered (see figure 11): hard-sphere correlation (dashed lines), high and low estimates of g measured from the x-ray data (dotted and thick lines, respectively).

TABLE III: A simple criterion for estimating how well the predictions of the different models agree with the experimental data: the relative mean squared differences between theoretical and experimental effective wavenumbers (average of the imaginary and real parts) over the 30-300 kHz frequency range. Different g functions are considered: from the hard-sphere approximation (hs), and from the measured correlation (see Fig. 11) with the lower (xp-) middle (xp) and upper (xp+) estimates.

Model	ISA	Keller			SCA				
g	/	hs	xp -	xp	xp +	hs	xp -	xp	xp +
(%)	14.8	11.3	7.3	12.4	17.7	10.1	4.3	10.8	19.6

or not the polydisperse correlations are sufficient to fully explain the discrepancy. Nonetheless, we find that plausible values for g are able to give good agreement. A more precise determination of the correlations would be necessary for a definitive conclusion to be drawn.

V. CONCLUSIONS

We have investigated wave propagation through a complex medium in which low-frequency scattering resonances lead to strong dispersion, with large peaks in the velocity and attenuation. By choosing to work with a relatively simple acoustic system – bubbles in the elastic medium PDMS – we have shown how these signatures of strong resonant scattering are influenced by the coupling between the scatterers. This leads to the breakdown of the independent scatterer approximation (ISA), which is commonly used to interpret experimental data. A crucial step in investigating the failure of the ISA in this system has been our ability to characterize the physical properties of bubbly PDMS very carefully, including independent measurements of the elastic properties of the matrix as well as the concentration and size distribution of the scatterers. Remarkably, we find that this failure of the ISA occurs even though the concentration of scatterers is low, only 2% in our case. It is worth noting one important consequence: if the ISA is used to estimate the size distribution of the scatterers, significantly smaller sizes are found than by direct imaging methods.

In this paper, we have proposed that this discrepancy can be explained by accounting for the role of correlations in the scatterers' positions, which we were able to probe directly using x-ray tomography. Following Keller's approach, we have shown that these correlations brought a non-negligible correction to the ISA, and that the agreement with the experimental data was improved, although not perfect. We have proposed an alternative approach, based on a self-consistent argument, with which we were able to take into account the effect of polydispersity on the correlations: bubbles of different radii are not correlated with their neighbours in the same way. Again, x-ray tomography allowed us to investigate this polydisperse correlation, which was found to be different from the monodisperse estimate: small bubbles are more likely to be close to other bubbles, whereas big bubbles are often isolated. We have shown that, within the possible polydisperse correlations that are consistent with our x-ray measurements, the SCA was able to provide a satisfactory explanation for the observed shift to higher frequencies in the acoustic resonances in the sample. It should also be noted that our model could be refined to account for more complex situations. In particular, when the correlations are long-range in a thin sample, one can expect the boundaries to play a role in the correlation, an effect we did not incorporate. Also, we looked at correlation effects or inhomogeneity effects, but we have not considered the case in which both effects are coupled.

An interesting question is the following: why are correlations important in the bubbly medium studied here, whereas they have not been detected before for bubbles in water [26] or bubbles in a yield stress fluid [8]? According to equation (17), the magnitude of the correction due to the positional correlations is proportional to the volume fraction of scatterers Φ , which was generally lower in pre-

vious studies (5×10^{-4} to 10^{-2} at most), so that β would be expected to be low. However, it is interesting to note that some previous studies did report deviations between Foldy's prediction and the experimental data that might be interpreted as a manifestation of correlation effects. In the historical data by Silberman [27], for instance, the measured attenuation was much larger than Foldy's estimate. Feuillade proposed that the discrepancy could be resolved by introducing an arbitrary fitting parameter [28] that one can interpret as a correlation length (see the appendix). Wilson *et al.* also observed deviations from Foldy's estimate, as their attenuation peak was at a lower frequency than what was expected from the size analysis (see Fig. 10 in [26]). They attributed this discrepancy to the uncertainty in their measurement of the bubble size distribution, but one can imagine that correlation effects were responsible for this shifting of the attenuation peak. Indeed, large depletion zones around bubbles have been observed in bubbly liquids [29], which would lead to positional correlations. In our sample, the exact mechanism leading to the positional correlations has not been identified unambiguously. Ostwald ripening might induce the disappearance of small bubbles close to bigger bubbles, hence leading to the isolated big bubbles we observed. Another possible scenario could involve the rotation of the cell when the sample was prepared. If one considers that only the buoyancy and the Stokes drag force are relevant (inertial forces were negligible in our set-up), a bubble is expected to move along a circle whose radius is inversely proportional to the rotation frequency, and proportional to the square of the bubble radius. The movement of the bubbles may induce hydrodynamic interactions leading to positional correlations. This hypothesis is supported by the observation of strong clustering when the cell was rotated at a lower speed (0.7 rpm), *i.e.*, when the radii of the circles followed by the bubbles were larger.

Acknowledgments

Support from the Natural Sciences and Engineering Research Council of Canada is gratefully acknowledged. The authors wish to thank A. Derode, M. Devaud, T. Hocquet, and J.-C. Bacri for numerous discussions, as well as R. Jayaraman for his help in enabling the x-ray experiments to be carried out.

Appendix A: Self-consistent approach for multiple scattering of waves

We propose a self-consistent approach for calculating the dispersion relation of a random multiply scattering medium, taking into account the positional correlations of the scatterers. Let us consider an infinite medium with n inclusions per unit volume. We limit ourselves to low frequencies such that the wavelength is large compared

to the size of the scattering inclusions, which means we can consider that the waves scattered by the inclusions are spherical: when scatterer i is excited by a wave with amplitude p_i , it generates a wave $p_i f_s^i \exp(ik_0 r)/r$ at distance r , where f_s^i is its scattering function and k_0 the wave number in the pure medium. The total field experienced by inclusion i , due to the other scatterers, is given by the self-consistent relation

$$p_i = \sum_{j \neq i} p_j f_s^j \frac{e^{ik_0 r_{ij}}}{r_{ij}}, \quad (\text{A1})$$

where r_{ij} is the distance between scatterers i and j . In the case of a finite number of scatterers, Eq. (A1) can be solved and all the p_i exactly computed. For an infinite number of inclusions, however, taking into account the full multiple scattering is a difficult task and the p_i are not easily accessible. In particular, the $1/r$ range of the interaction means that no pair (i, j) can be neglected *a priori* in Eq. (A1).

Let us further simplify the problem by assuming that all the scatterers are identical ($f_s^i = f_s$) and look for modes that take the form of plane waves propagating in the x direction: $p_i = P \exp(ikx_i)$, where k is the effective wave number we want to determine, and P the amplitude of the mode. Then, Eq. (A1) reduces, for scatterer $i = 0$ arbitrarily chosen as the central one located at $r = 0$, to

$$1 = \sum_{j \neq 0} e^{ikx_j} f_s \frac{e^{ik_0 r_j}}{r_j} = f_s \sum_{j \neq 0} \frac{e^{i(kr_j \cos \theta_j + k_0 r_j)}}{r_j}, \quad (\text{A2})$$

where r_j is the distance to scatterer j , and θ_j the angle between the direction of propagation and the position of scatterer j (see Fig. 13).

One can approximate the discrete equation by a continuous equation, taking into account the positional correlations with the pair correlation function $g(r)$:

$$1 = f_s \int d^3 r \times n g(r) \frac{e^{i(kr \cos \theta + k_0 r)}}{r} \quad (\text{A3a})$$

$$= \frac{4\pi n f_s}{k} \int_0^\infty n g(r) \sin(kr) e^{ik_0 r} dr. \quad (\text{A3b})$$

Invoking a small imaginary part of k_0 to preserve the convergence of the integral, one can then calculate the effective wave number:

$$k^2 = k_0^2 + \frac{4\pi n f_s}{1 + 4\pi n f_s \int (1 - g(r)) \frac{\sin kr}{k} e^{ik_0 r} dr}. \quad (\text{A4})$$

Note that equation (A4) reduces to Foldy's equation if the denominator is approximated by 1, and to Keller's equation if it is expanded to second order in $n f_s$. Interestingly, it has some similarities with the equation proposed by Feuillade, which was found to give excellent agreement

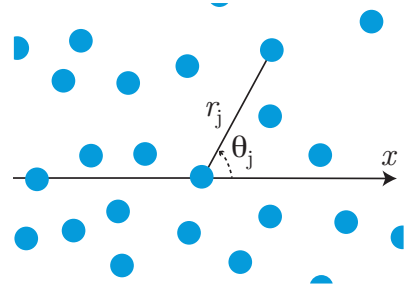


FIG. 13: (Color online) An infinite 3D medium with spherical scatterers is considered. The position of scatterer 0 is arbitrarily chosen as the centre of the coordinates and we look for modes of the system consisting of plane waves propagating in the x direction. The dispersion relation is obtained by calculating the total field experienced by scatterer 0 due to the other scatterers.

with experimental data for bubbly liquids (see equation (30) in [30]). Feuillade's model has been subject to criticisms [13, 31], in particular because, for unclear reasons, it assumes that the interactions between the scatterers are confined within a finite range. It might be that this finite range is related to correlations. Note that the approach we develop here is similar to Feuillade's. The differences are that (1) we abandon the assumption that all the scatterers are in phase, which is true only locally, and (2) we include the positional correlations.

For a polydisperse assembly of scatterers, the same self-consistent scheme can be used. In this case, the total field p_i depends *a priori* on the radius of the bubble, $p_i = P(R_i) \exp(ikx_i)$, meaning that equation (A3a) must be generalized into

$$P(R) = f_s(R) \int n(R') dR' P(R') \times \int g(r, R, R') \frac{e^{i(kr \cos \theta + k_0 r)}}{r} d^3 r, \quad (\text{A5})$$

where $g(r, R, R')$ gives the probability of finding a bubble with radius R' at a distance r from a central bubble with radius R . In the general case, equation (A5) cannot be directly simplified into a dispersion relation. However, if we assume that the correlation does not depend on R' ($g(r, R, R') = g(r, R)$), a further integration over R yields

$$1 = \int n(R) f_s(R) dR \int g(r, R) \frac{e^{i(kr \cos \theta + k_0 r)}}{r} d^3 r \quad (\text{A6})$$

from which we obtain the dispersion relation

$$k^2 = k_0^2 + \frac{\int 4\pi n(R) f_s(R) dR}{1 + A}, \quad (\text{A7})$$

with

$$A = \int 4\pi n(R) f_s(R) dR \int (1 - g(r, R)) \frac{\sin kr}{k} e^{ik_0 r} dr.$$

Note that, as in the ISA, polydispersity modifies the equation by changing nf_s into $\int n(R)dRf_s(R)$. But polydispersity also brings another non-trivial modification: the correlation can depend on the radius of the cen-

tral bubble considered, which makes different correlations possible for different bubble sizes, as in our bubbly sample.

-
- [1] J. B. Pendry, Phys. Rev. Lett. **85**, 3966 (2000).
- [2] Z. Liu, X. Zhang, Y. Mao, Y. Y. Zhu, Z. Yang, C. T. Chan, and P. Sheng, Science **289**, 1734 (2000).
- [3] D. R. Smith, J. B. Pendry, and M. C. K. Wiltshire, Science **305**, 788 (2004).
- [4] Z. Yang, J. Mei, M. Yang, N. Chan, and P. Sheng, Phys. Rev. Lett. **101**, 204301 (2008).
- [5] V. N. Alekseev and S. A. Rybak, Acoustical Physics **45**, 535 (1999).
- [6] E. A. Zabolotskaya, Y. A. Ilinskii, G. D. Meegan, and M. F. Hamilton, J. Acoust. Soc. Am. **118**, 2173 (2005).
- [7] A. Strybulevych, V. Leroy, M. G. Scanlon, and J. H. Page, Soft Matter **3**, 1388 (2007).
- [8] V. Leroy, A. Strybulevych, J. H. Page, and M. G. Scanlon, J. Acoust. Soc. Am. **123**, 1931 (2008).
- [9] V. Leroy, A. Strybulevych, M. G. Scanlon, and J. H. Page, Eur. Phys. J. E **29**, 123 (2009).
- [10] P. Sheng, *Introduction to Wave Scattering, Localization and Mesoscopic Phenomena* (Academic Press, New York, 1995).
- [11] L. L. Foldy, Physical Review **67**, 107 (1945).
- [12] J. Keller, Proc. Symp. Appl. Math. **16**, 145 (1964).
- [13] F. S. Henyey, J. Acoust. Soc. Am. **105**, 2149 (1999).
- [14] M. Haney and R. Snieder, Phys. Rev. Lett. **91**, 093902 (2003).
- [15] A. Prosperetti, J. Acoust. Soc. Am. **61**, 17 (1977).
- [16] B. Liang and J.-C. Cheng, Phys. Rev. E **75**, 016605 (2007).
- [17] A. B. Wood, *A Textbook of sound* (Bell, London, 1932).
- [18] P. Y. Longin, C. Verdier, and M. Piau, J. Non-Newtonian Fluid Mech. **76**, 213–232 (1998).
- [19] V. Leroy, K. M. Pitura, M. G. Scanlon, and J. H. Page, J. Non-Newtonian Fluid Mech. **165**, 475 (2010).
- [20] A. Strybulevych, V. Leroy, M. G. Scanlon, and J. H. Page, in *Proceedings of Symposium on Ultrasonic Electronics* (2009), pp. 395–396.
- [21] F. Schneider, T. Fellner, J. Wilde, and U. Wallrabe, J. Micromech. Microeng. **18**, 1 (2008).
- [22] C. G. Delides and T. A. King, J. Chem. Soc., Faraday Trans. 2 **75**, 359 (1979).
- [23] V. Leroy, Y. Fan, A. L. Strybulevych, G. G. Bellido, J. H. Page, and M. G. Scanlon, in *Bubbles in Food 2: Novelty, Health and Luxury*, edited by G. M. Campbell, M. G. Scanlon, and D. L. Pyle (AACC Press, St Paul, 2008).
- [24] L. M. Brekhovskikh, *Waves in layered media* (Academic press, New York, 1960).
- [25] A. Derode, V. Mamou, and A. Tourin, Phys. Rev. E **74**, 036606 (2006).
- [26] P. S. Wilson, R. A. Roy, and W. M. Carey, J. Acoust. Soc. Am. **117**, 1895 (2005).
- [27] E. Silberman, J. Acoust. Soc. Am. **29**, 925 (1957).
- [28] C. Feuillade, J. Acoust. Soc. Am. **99**, 3412 (1996).
- [29] A. Cartellier and N. Rivière, Phys. Fluids **13**, 2165 (2001).
- [30] C. Feuillade, J. Acoust. Soc. Am. **102**, 1242 (1997).
- [31] Z. Ye, J. Acoust. Soc. Am. **102**, 1239 (1997).